

pubs.acs.org/Macromolecules Article

Charged Polymers: From Polyelectrolyte Solutions to Polyelectrolyte Complexes

Ryan Sayko, Yuan Tian, Heyi Liang, and Andrey V. Dobrynin*



Cite This: Macromolecules 2021, 54, 7183-7192



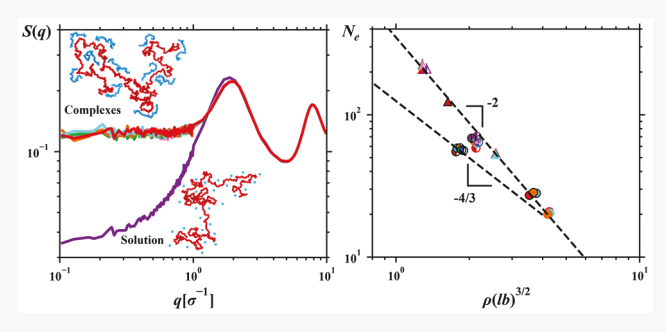
ACCESS

Metrics & More

Article Recommendations

Supporting Information

ABSTRACT: Coarse-grained molecular dynamics simulations, random phase approximation (RPA) approach, and scaling analysis are used to study static and dynamic properties of concentrated polyelectrolyte solutions of positively charged chains with the degree of polymerization N_+ = 400 and their mixtures with negatively charged chains with degrees of polymerization N_- varying between 10 and 400. Simulations show that both the effective chain Kuhn length and mean-square end-to-end distance of a chain decrease with increasing monomer concentration, pointing out screening of the electrostatic interactions by surrounding chains. The structure factor S(q) has a characteristic



peak at intermediate wavenumbers q^* which location moves toward smaller q values with decreasing monomer concentration. It is demonstrated that the plateau in S(q) at a small q is controlled by system compressibility and increases with increasing degree of polymerization of negatively charged chains. These results are in agreement with S(q) calculated in the framework of the RPA approach considering a solution of neutral chains as a reference system. In the framework of this approach, the location of the maximum in the scattering function at q^* scales with monomer concentration as $\rho^{-0.25}$. Analysis of the chain dynamics in the mixtures of oppositely charged chains shows that chain relaxation is a combination of constraint release and chain reptation processes. Constraint release is demonstrated to be the dominant mechanism in mixtures with negatively charged chains having intermediate degrees of polymerization. The degree of polymerization N_e between entanglements of the tube and super tube for charged systems is found to scale with concentration as $N_e \sim \rho^{-2}$ with corresponding packing numbers $P_e = 18.45 \pm 0.93$. This is in contrast with mixtures of neutral chains, where in addition to $N_e \sim \rho^{-2}$ scaling, the degree of polymerization between entanglements of the super tube follows scaling $N_e \sim \rho^{-4/3}$ with packing number $N_e = 6.64 \pm 0.19$.

■ INTRODUCTION

The last half century saw an unprecedented growth of research dealing with properties of charged polymers-macromolecules with ionizable groups, which upon dissociation in a solvent with high dielectric permittivity release counterions into solution, leaving charged groups on the polymer backbones. 1-10 Solution properties of such polymers are manifestations of a fine interplay between electrostatic interactions, polymer-solvent affinity, and chain conformational entropy. This interplay culminates in the appearance of a characteristic length scale called the electrostatic blob, starting from which electrostatic interactions become a dominant force responsible for chain stretching. In dilute salt-free polyelectrolyte solutions, this results in a linear increase in the chain size $R \sim N$ with its degree of polymerization (DP) N and a crossover monomer concentration c^* to a semidilute solution regime to demonstrate a strong N dependence such that $c^* \sim N^{-2}$. Numerical prefactors in the scaling expressions depend on the fraction of ionized groups, solvent dielectric permittivity, and solvent quality for the polymer backbone. In semidilute solutions of overlapping chains, electrostatic interactions are screened on length scales larger than the solution correlation length with chain statistics to be that of a flexible chain with an effective Kuhn length on the order of solution correlation length. On length scales smaller than the correlation length, sections of the chain remain stretched by unscreened electrostatic repulsions between ionized groups.^{3,5,7}

Replacing counterions with multivalent ions (i.e., Ca^{2^+} and Fe^{3+}) or by oppositely charged polyelectrolytes promotes chain complexation, associations, and/or collapse.^{6,8–16} In particular, in the case of mixtures of oppositely charged chains, electrostatic interactions between charged groups drive chains' complexation and collapse with complex size in a dilute solution increasing with the degree of polymerization as $R \sim N^{1/3}$. Equilibrium monomer density is determined by optimization of the excluded volume interactions and

Received: May 30, 2021 **Revised:** June 23, 2021 **Published:** July 22, 2021





fluctuation-induced electrostatic attraction with a characteristic length scale of the density fluctuations having similar dependence on the system parameters as an electrostatic blob size. An increase in polymer concentration results in a phase separation into a concentrated phase made of an electroneutral mixture of oppositely charged chains and a dilute phase of charge-balanced polyelectrolyte (PE) complexes. The addition of salt screens electrostatic interactions by decreasing the solubility of polyelectrolytes in solutions with monovalent counterions while promoting the solubility of the PE complexes broadening a single-phase concentration regime. 8–11

Electrostatic interactions significantly influence the dynamics of charged polymers as well. S,17-21 In salt-free polyelectrolyte solutions, they suppress the chain entanglement broadening regime with unentangled chain dynamics such that the entanglement concentration $c_{\rm e}$ could be 2-3 orders of magnitude above the overlap concentration c^* . It turns out that, for polyelectrolyte systems studied so far, chains begin to entangle only at high polymer concentrations corresponding to the concentration regime of overlapping electrostatic At these concentrations, polymer dynamics is similar to that in solutions of neutral polymers with electrostatic interactions treated as perturbations.⁴ A similar behavior is observed in solutions of oppositely charged chains. In this case, the high concentration branch of the coexistence curve corresponds to a concentrated solution regime. 9,11,24 At these concentrations, the electrostatic attractions between oppositely charged chains, causing system phase separation and defining equilibrium monomer density, are weak at length scales comparable to the size of electrostatic blobs in polyelectrolyte solutions. Their effect on chains' dynamics is reduced to renormalization of the effective monomeric friction coefficient and monomer relaxation time such that the chains follow ideal chain dynamics with renormalized monomeric properties. 25,26

However, despite a general understanding of the properties of charged polymers outlined above, the complete picture of concentrated solutions of oppositely charged polyelectrolytes with different chain DPs and polyelectrolyte solutions with univalent counterions is still missing. To fill this void, we use coarse-grained molecular dynamics simulations to study chain conformations, scattering function, and chains' reptation dynamics. The scattering results are analyzed using the static structure factor calculated in the framework of the random phase approximation (RPA) approach by considering a neutral system as a reference state. The chains' dynamics is analyzed by monitoring the mean-square displacement of the central monomers on the polymer backbone and the chain's center of mass to determine the effect of constraint release on the chains' dynamics as DP asymmetry between polyelectrolytes increases. We begin our discussion with a brief overview of the coarse-grained model used in molecular dynamics simulations.

MODEL AND SIMULATION DETAILS

We performed molecular dynamics simulations of polyelectrolytes and mixtures of oppositely charged polyelectrolytes in the concentrated solution regime and in a melt. In our simulations, polyelectrolytes were modeled as bead-spring chains consisting of 400, 200, 100, 50, 20, and 10 beads (monomers) and each carrying either a positive or negative unit charge (see Figure 1). Counterions are represented by beads with diameter σ . The beads interacted through a

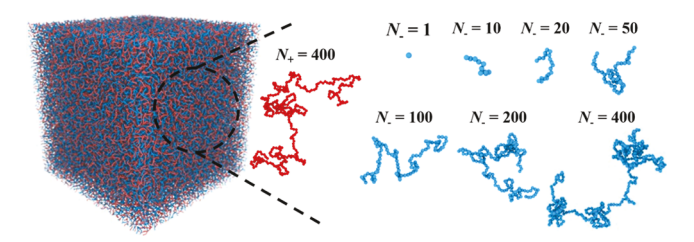


Figure 1. Snapshots of the simulation box and positively charged chains with the degree of polymerization $N_{+}=400$ and negatively charged chains (counterions) of different degrees of polymerization N.

truncated-shifted Lennard-Jones (LJ) potential with the interaction parameter ε and Coulomb potential with the Bjerrum length $l_{\rm B} = 1.0\sigma$. The connectivity of monomers into chains was maintained by the combination of the finite extensible nonlinear elastic (FENE) and truncated-shifted LJ potentials.²⁷ The FENE potential spring constant was set to 30 ε/σ^2 and maximum bond length $R_{\rm max}=1.5\sigma$. In addition, an angular potential was introduced between neighboring backbone bonds with the bending constant $k_{\theta} = 1.5\varepsilon$ to reduce the degree of polymerization between entanglements. In all simulations, the temperature was set to $T = \varepsilon/k_{\rm B}$ ($k_{\rm B}$ is the Boltzmann constant, and T is the absolute temperature). Simulations of polyelectrolyte solutions and mixtures of positively and negatively charged chains with degrees of polymerization N_+ and N_- were performed at total bead (monomer) densities $\rho \sigma^3 = 0.85$ and 0.26 by following the procedure described in the Supporting Information. Note that these two different bead densities correspond to melt and concentrated solution, respectively. The lower bead concentration $\rho \sigma^3 = 0.26$ corresponds to a high density branch of the phase coexistence curve for a symmetric system with $N_+ = N_-$ = 400 obtained by setting the system pressure to $P = 0 k_B T / \sigma^3$. The following systems consisting of (N_+, N_-) pairs with equal densities of each type of monomers were studied: (400, 400), (400, 200), (400, 100), (400, 50), (400, 20), (400, 10), and (400, 1). A system with (400, 1) represents a polyelectrolyte solution.

RESULTS AND DISCUSSION

Chain Size and Kuhn Length. We begin our discussion of solution properties with an analysis of chain conformations. Figure 2 shows simulation results for the mean-square end-toend distance of a section of the chain with s bonds, $\langle R_e^2(s) \rangle$. The two plots look almost identical with a larger spread of the data and a larger chain size for systems at a lower density. This should not be surprising since, at low bead concentrations, the correlation blobs describing screening of the electrostatic interactions are larger in size. Furthermore, we see two characteristic regimes in chain size s dependence. At short distances along the polymer backbone, the mean-square endto-end distance increases quadratically with the number of bonds in a section of the chain, $\langle R_e^2(s) \rangle \propto s^2$. This takes place at distances smaller than the chain Kuhn length. This regime is followed by the $\langle R_e^2(s) \rangle \propto s$ regime describing a random walk. This occurs for the number of bonds s > 10.

To quantify the effect of the local chain stiffening, we study the decay of the orientational correlations between unit bond vectors \mathbf{n}_i and \mathbf{n}_{i+s} pointing along chain bonds and separated by s bonds defined as

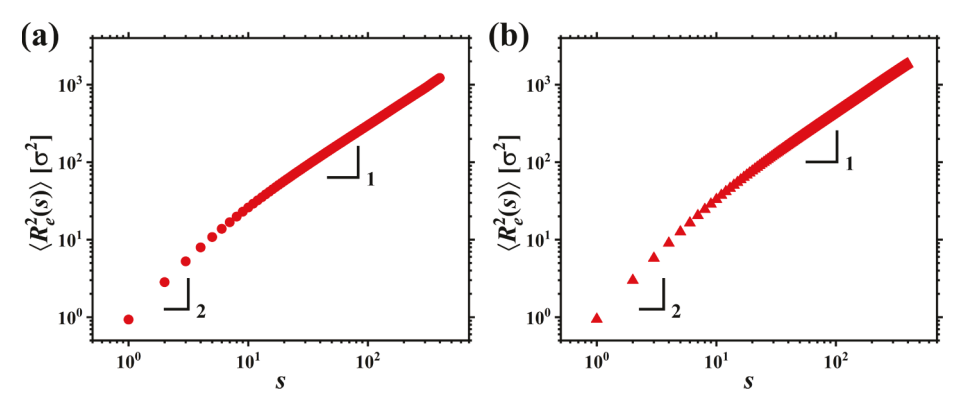


Figure 2. Dependence of the mean-square end-to-end distance of the section of the polyelectrolyte chain $(N_+ = N_- = 400)$ with s bonds for systems with bead densities $\rho\sigma^3 = 0.85$ (a) and $\rho\sigma^3 = 0.26$ (b).

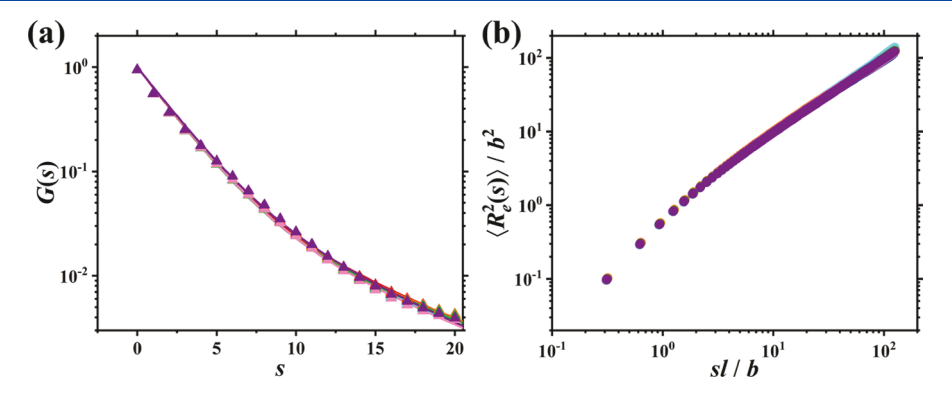


Figure 3. (a) Bond—bond correlation function for polymer systems with bead concentration $\rho\sigma^3 = 0.26$. The solid line is the best fit to eq 2. (b) Dependence of the normalized chain size $\langle R_e^2(s)\rangle/b^2$ on the number of Kuhn segments per chain segment sl/b. Symbol notations for each system are given in Table 1.

Table 1. Parameters for Charged Systems with $N_+ = 400$

N_	b [σ]	$q^*[\sigma^{-1}]$	$S(0)[\sigma^{-3}]$	$N_{ m e}$	$P_{\rm e}$	$N_{ m e,+}$	$P_{\mathrm{e},+}$	Symbol
$ ho\sigma^3=0.85$								
400	3.05 ± 0.08	3.00	0.009	20.83±0.11	19.44	62.07±0.83	16.78	•
200	3.06 ± 0.19	3.00	0.009	20.38±0.13	19.32	63.36±1.66	17.03	
100	3.02 ± 0.22	3.00	0.009	19.99±0.22	18.76	65.28±2.25	16.95	•
50	3.06 ± 0.16	3.00	0.009			67.16±1.40	17.54	•
20	3.10 ± 0.10	3.00	0.009			64.10±1.30	17.47	
10	3.08 ± 0.21	3.00	0.009			67.22±0.66	17.72	
1	3.07 ± 0.08	3.26	0.0075			70.49±3.90	18.05	•
				$\rho\sigma^3=0.26$				
400	4.75 ± 0.22	1.96	0.13	53.64±1.06	18.83	208.37±17.80	18.56	A
200	4.75 ± 0.24	1.96	0.13	52.55±1.03	18.64	226.15±11.82	19.33	A
100	4.76 ± 0.22	1.96	0.13			221.76±8.26	19.21	A
50	4.75 ± 0.23	1.96	0.13			225.19±13.40	19.29	A
10	4.76 ± 0.25	1.96	0.13			222.52±9.12	19.24	
1	4.88 ± 0.28	1.87	0.035			209.58±12.55	19.38	

$$G(s) = \frac{1}{n_{b} - s} \sum_{i=1}^{n_{b} - s} \langle \mathbf{n}_{i} \cdot \mathbf{n}_{i+s} \rangle$$
(1)

where $n_b = N_j - 1$ is the number of bonds in the polyelectrolyte chain and the brackets $\langle ... \rangle$ denote averaging over chain configurations. The end effects are eliminated by omitting contributions from 20 bonds on each chain end in calculations of the bond-bond correlation function (eq 1).

Figure 3 illustrates a typical bond—bond correlation function obtained in our simulations. In charged polymer systems, there are two effects that contribute to the local chain stiffening: chain tension and bending deformation mode.²⁸ To account for these effects, the bond—bond correlation function is approximated by the double-exponential function of the following form^{28,29}

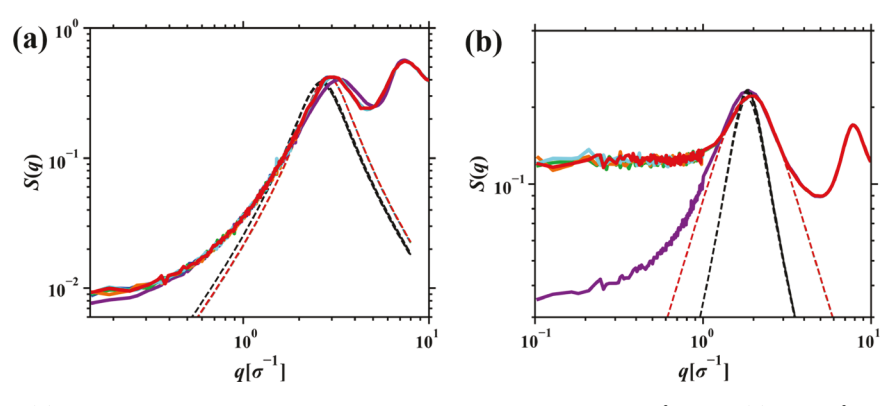


Figure 4. Structure factor S(q) for systems of polyelectrolyte chains with bead concentrations $\rho\sigma^3=0.85$ (a) and $\rho\sigma^3=0.26$ (b). Lines of different colors represent systems with counterions or solvent chains having DPs equal to 400 (red), 200 (light blue), 100 (orange), 50 (green), 20 (blue), 10 (pink), and 1 (purple). The dashed lines correspond to eq 14 using the bond length l and Kuhn length b obtained from neutral system analysis with value $v(\delta_+ - \delta_-)^2$ as fitting parameters that are equal to $10.5\sigma^3$ and $25.3\sigma^3$ in panels (a, b), respectively. The color dashed lines show the best fit to eq 17 with values of the fitting parameters $(C, B, v(\delta_+ - \delta_-)^2)$ equal to $(0.9\sigma^5, 58.2\sigma, 11.8\sigma^3)$ for $\rho\sigma^3 = 0.85$ and $(1.0\sigma^5, 13.5\sigma, 2.9\sigma^3)$ for $\rho\sigma^3 = 0.26$.

$$G(s) = (1 - \alpha)e^{-|s|/\lambda_1} + \alpha e^{-|s|/\lambda_2}$$
(2)

where α , λ_1 , and λ_2 are fitting parameters. The two mechanisms of chain deformation are represented by correlation lengths λ_1 and λ_2 . With the given bond—bond correlation function, the mean-square end-to-end distance of a chain section with s bonds is written as

$$\langle R_{e}^{2}(s) \rangle = \frac{1}{N-s} \sum_{i=1}^{N-s} \left\langle l^{2} \left(\sum_{j=i}^{i+s-1} \mathbf{n}_{j} \right)^{2} \right\rangle$$
$$= l^{2} ((1-\alpha)g(\lambda_{1}, s) + \alpha g(\lambda_{2}, s)) \tag{3}$$

where l is the bond length and function $g(\lambda_s s)$ is defined as

$$g(\lambda, s) = s \frac{1 + e^{-1/\lambda}}{1 - e^{-1/\lambda}} - 2e^{-1/\lambda} \frac{1 - e^{-s/\lambda}}{(1 - e^{-1/\lambda})^2}$$
(4)

The Kuhn length b is calculated from the fitting parameters of the bond—bond correlation function

$$b = \frac{\langle R_{\rm e}^2(s) \rangle}{sl} \bigg|_{s \to \infty} = l((1 - \alpha)h(\lambda_1) + \alpha h(\lambda_2))$$
(5)

where function $h(\lambda)$ is

$$h(\lambda) = \frac{1 + e^{-1/\lambda}}{1 - e^{-1/\lambda}} \tag{6}$$

Figure 3a represents the bond—bond correlation function for systems with different degrees of polymerization N_- . The Kuhn lengths obtained from the analysis of the fitting results are summarized in Table 1 for bead concentrations $\rho\sigma^3 = 0.85$ and 0.26. Calculated values of the Kuhn length in charged systems appear to be larger than those for solutions of neutral polymers at the same bead density (see the Supporting Information). For comparison, the bare Kuhn length in noninteracting systems is equal to $b = 2.46\sigma$. This points out that electrostatic interactions between charges stiffen polymer chains. We can use these values of the Kuhn lengths to represent data in terms of the number of Kuhn segments per chain section by plotting $\langle R_{\rm e}^2(s) \rangle/b^2$ as a function of sl/b (see Figure 3b). It follows from this plot that the crossover between

the two different scaling laws of chain size dependence occurs at $sl \sim b$, as expected.

Structure Factor. The static structure factor S(q) is defined as

$$S(q) = \frac{1}{V} \sum_{i=1}^{N_b} \sum_{j=1}^{N_b} f_j f_j \langle \exp[-i\mathbf{q} \cdot (\mathbf{R}_i - \mathbf{R}_j)] \rangle$$
(7)

where q is the scattering vector and f_i is the form factor of the ith bead located at a point with the radius vector R_i . The summation in eq 7 is performed over all beads $N_{\rm b}$ in a system, and brackets $\langle \rangle$ denote the ensemble averaging. To calculate the structure factor of polyelectrolyte solutions, the monomer form factors were set to $f_+ = 1.0$ for positively charged beads and $f_- = 0$ for negatively charged beads.

Figure 4a,b shows the structure factor S(q) for polyelectrolyte solutions calculated by using a hybrid of the fast Fourier transform (FFT)-based approach developed in ref 28 and direct calculations of S(q) for monomer distances $r < r_{cut} =$ $2\pi\sigma$. There are two characteristic peaks in the structure factor S(q). The intermediate q-peak corresponds to the charged density fluctuations. Its location remains unchanged for N varying between 10 and 400 with $q^*\sigma \approx 1.96$ and 3.0 for systems with bead concentrations $\rho \sigma^3 = 0.26$ and 0.85, respectively. For polyelectrolyte solutions $(N_{-} = 1)$, the corresponding peak locations are $q^*\sigma \approx 1.87$ and 3.26. The second peak located at $2\pi/l$ corresponds to correlated scattering from neighboring beads along the chain separated by bonds with lengths $l \approx 0.96\sigma$ and 0.97σ for bead concentrations $\rho \sigma^3 = 0.85$ and 0.26, respectively. The saturation of structure factor S(q) at a small q represents the suppression of bead density fluctuations due to electroneutrality requirements. For polyelectrolyte solutions with $N_{-} = 1$, $S(0) \approx 0.0075\sigma^{-3}$, while for the mixtures of polyelectrolytes, we see the saturation at $S(0) \approx 0.009 \sigma^{-3}$ for $N_{-} > 10$ and bead concentration $\rho \sigma^3 = 0.85$. The larger values, $S(0) \approx 0.13\sigma^{-3}$ for $N_{-} > 10$ and $S(0) \approx 0.035\sigma^{-3}$ for $N_{-} = 1$, are observed for $\rho\sigma^3 = 0.26$, indicating a higher degree of the system compressibility.

To explain this peculiar behavior of the structure factor S(q), we use random phase approximation (RPA)^{4,11,30–33} to describe bead density fluctuations. In this approximation, the matrix G(q) of the pair correlation functions is written in terms

of the matrix of structural correlation functions $\mathbf{g}(q)$ describing the arrangement of beads into polymer chains, the matrix of electrostatic interactions V(q), and the matrix of the direct correlation functions $\mathbf{C}(q)$ representing short-range interactions between beads^{30–33}

$$\mathbf{G}^{-1}(q) = \mathbf{g}^{-1}(q) + V(q) - C(q)$$
 (8)

Matrix $\mathbf{g}(q)$ is a diagonal matrix, $\mathbf{g}_{\alpha}(q)\delta_{\alpha\beta}$, with functions $\mathbf{g}_{\alpha}(q)$ for chains with $N\neq 1$ given by the Debye function

$$g_{\alpha}(q) = 2\rho_{\alpha}N_{\alpha}(e^{-q^{2}R_{\alpha}^{2}} + q^{2}R_{\alpha}^{2} - 1)/(q^{2}R_{\alpha}^{2})^{2}$$
(9)

where $R_{\alpha}^2 \equiv lbN_{\alpha}/6$. In the case of N=1, the function $g_{\alpha}(q)=\rho_{\alpha}$. The matrix of electrostatic interactions has the following form

$$V(q) = 4\pi l_{\rm B} z^{\rm T} z/q^2 \tag{10}$$

where the charge valence vector z = (1, -1) and z^T is its transpose.

The elements of the matrix of the direct correlation functions describe correlations in a reference monomeric system

$$\mathbf{C}(q) = \nu \boldsymbol{\delta}^T \boldsymbol{\delta} + c(\rho) \mathbf{e}^T \mathbf{e}$$
 (11)

where vector $\mathbf{e}=(1,1)$, \mathbf{e}^T is its transpose, vector $\boldsymbol{\delta}=(\delta_+,\delta_-)$ with the corresponding transpose vector $\boldsymbol{\delta}^T$, and $\boldsymbol{\nu}$ is the monomer excluded volume. The values of parameters δ_i account for asymmetry in the packing of monomers and counterions as well as renormalization of the short-range interactions due to charge density fluctuations. This effect is well known in the block copolymer systems where fluctuation corrections renormalize the Flory–Huggins χ -parameter shifting the microphase separation transition to lower temperatures. In the framework of the lattice model for a reference monomeric system of beads, $c(\rho)$ describes the repulsive part of interaction potential with the excluded volume $\boldsymbol{\nu}$ and can be approximated as 33,37

$$c(\rho) = -\frac{\nu}{1 - \rho\nu} \tag{12}$$

The calculations of the structure factor S(q) with scattering amplitudes $f_+=1$ and $f_-=0$ are reduced to calculations of the element $G_{++}(q)$ of the matrix $\mathbf{G}(q)$

$$S(q) = G_{\perp \perp}(q) \tag{13}$$

The inversion of the matrix $\mathbf{G}^{-1}(q)$ is described in the Supporting Information. Below, we present the results for two limiting cases $q \approx q^*$ and $q \to 0$. To establish the dependence of the peak location q^* on the system parameters, we assume that $\rho v \approx 1$, which corresponds to incompressible mixtures. In this case, density fluctuations of positively and negatively charged monomers are interrelated, $\delta \rho_+(q) = -\delta \rho_-(q)$, and the function $G_{++}(q)$ reduces to

$$G_{++}(q) \approx \left(g_{+}^{-1}(q) + g_{-}^{-1}(q) + \frac{16\pi l_{\rm B}}{q^2} - \nu(\delta_{+} - \delta_{-})^2\right)^{-1}$$
(14)

For systems with $N_- \neq 1$, near the peak position $qR_\alpha \gg 1$, which results in $g_+^{-1}(q) \approx g_-^{-1}(q) \approx q^2 lb/6\rho$. Taking this into account, the peak location corresponds to the minimum of the function

$$G_{++}^{-1}(q) \approx \frac{q^2 lb}{3\rho} + \frac{16\pi l_{\rm B}}{q^2} - \nu(\delta_+ - \delta_-)^2$$
 (15)

and is estimated to be

$$q^* \approx (48\pi l_{\rm B}\rho/lb)^{1/4} \tag{16}$$

In the case of monovalent counterions $(N_{-} = 1)$, the term $g_{-}^{-1}(q) = \rho_{-}^{-1}$ in eq 15 is q-independent. This shifts the location of q^* for incompressible systems to the right by a factor of $2^{1/4}$, keeping the q^* dependence on the system parameters unchanged. The position of the peak obtained using eq 15 shows better agreement with simulation results for systems with lower bead density $\rho \sigma^3 = 0.26$, while for higher bead density $\rho \sigma^3 = 0.85$, there is a difference in peak locations (see Figure 4b). The appearance of the non-zero term $\nu(\delta_+ - \delta_-)^2$ reflects the renormalization of short-range interactions by the charge density fluctuations coupled through the third- and fourth-order terms in the free energy expansion in a power series of bead density fluctuations. However, even this correction cannot fully account for the renormalization of system parameters due to the strong coupling between density fluctuations. To highlight this effect, we use the phenomenological form of the correlation function close to the minimum

$$G_{++}^{-1}(q) \approx Cq^2 + \frac{B}{q^2} - \nu(\delta_+ - \delta_-)^2$$
 (17)

and consider C, B, and $v(\delta_+ - \delta_-)^2$ as fitting parameters. The best fits to this function are shown by the colored dashed lines in Figure 4. To derive relationships between these fitting parameters and bare charged polymer properties, one has to go beyond the RPA and apply the formalism developed in ref 38 based on the Brazovskii–Fredrickson–Helfand approximation. 34,39 This will be addressed in future publications.

The plateau value of the structure factor at $q \to 0$ and neglecting the δ -term is estimated as

$$S(0) \approx \frac{\rho}{2} ((N_{+}^{-1} + N_{-}^{-1}) + 2\rho \nu / (1 - \rho \nu))^{-1}$$
(18)

According to this expression, there is a monotonic decrease in the plateau values with decreasing the degree of polymerization N_{-} of negatively charged chains consistent with the trends observed in Figure 4.

Entanglements and System Dynamics. In concentrated solutions of chains with two different degrees of polymerization, there are two different types of entanglements: (i) entanglements formed between longer positively charged chains $N_{\rm c,+}$ forming a super tube that is renewed on time scales on the order of

$$\tau_{\rm L} \approx \tau (N_{\rm e,+}) (N_{\rm +}/N_{\rm e,+})^3$$
 (19)

with $\tau(N_{\mathrm{e},+})$ being the relaxation time of the polymer strand of the longer chains with DP = $N_{\mathrm{e},+}$ and (ii) entanglements formed by all chains with a degree of polymerization of a strand between entanglements DP = N_{e} that are renewed on the time scale on the order of relaxation time of the short chains

$$\tau_{\rm S} \approx \tau_0 N_-^3 / N_{\rm e} \tag{20}$$

with τ_0 being the characteristic monomeric time scale. These two different types of entanglements define two different tube relaxation mechanisms: constraint release controlled by the relaxation time of the short chains and

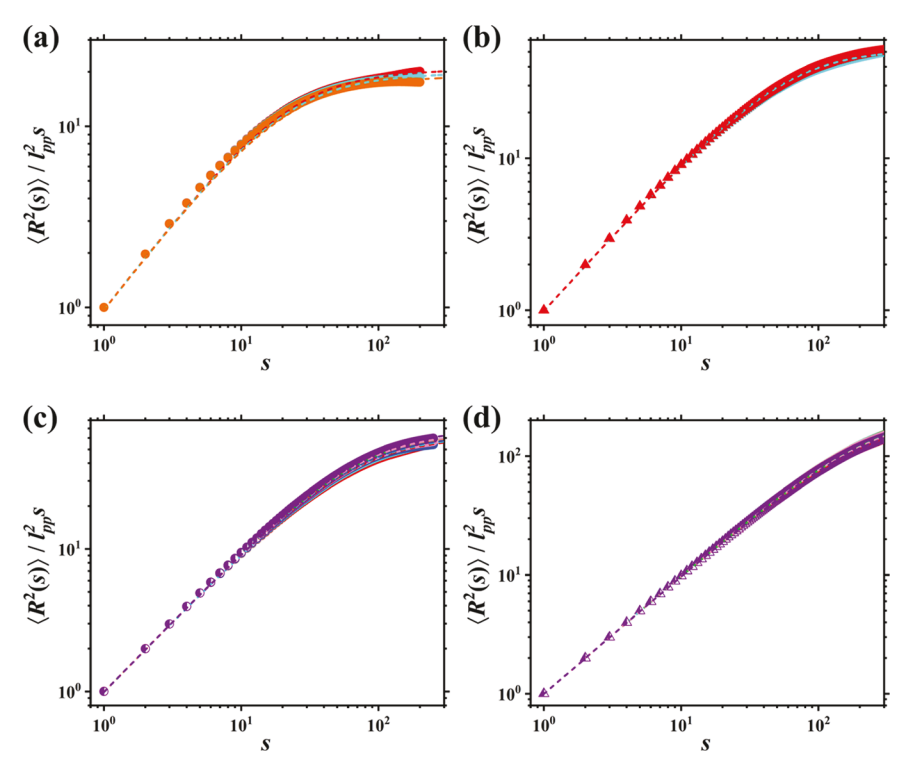


Figure 5. Dependence of the normalized mean-square end-to-end distance of the section of the primitive path chain with s bonds, $\langle R_{\rm e}^2(s) \rangle/l_{\rm pp}^2 s$, obtained for charged polymer systems with bead densities $\rho \sigma^3 = 0.85$ (a) and $\rho \sigma^3 = 0.26$ (b). Super tube parameters: normalized mean-square end-to-end distance of the section of the N_+ primitive path chain with s bonds, $\langle R_{\rm e}^2(s) \rangle/l_{\rm pp}^2 s$, obtained for charged polymer systems with bead densities $\rho \sigma^3 = 0.85$ (c) and $\rho \sigma^3 = 0.26$ (d). See Table 1 for symbol notations. Left-filled symbols correspond to super tube data.

renewal of the super tube confining motion of the longer chains.

For short chains with degrees of polymerization $N_- \geq N_{\rm e,+}$, relaxation time $\tau(N_{\rm e,+}) \leq \tau_{\rm S}$ and long chains reptate within a tube with the entanglement degree of polymerization $N_{\rm e}$. For the intermediate range of the degrees of polymerization of short chains, $N_{\rm e} \leq N_- < N_{\rm e,+}$, the confining tube formed by short chains restricting long-chain motion is renewed on the time scale on the order of reptation time of the short chains such that $\tau_{\rm S} < \tau(N_{\rm e,+})$. In this case, the relaxation time of the polymer strand with DP = $N_{\rm e,+}$ belonging to the long chains can be estimated as that of a Rouse chain of $N_{\rm e,+}/N_-$ blobs with blob relaxation time $\tau_{\rm S}$, $\tau(N_{\rm e,+}) \approx \tau_{\rm S}(N_{\rm e,+}/N_-)^2$. Taking this into account, we obtain the following expression for the reptation time of long chains

$$\tau_{\rm L} \approx \tau_0 N_- N_+^3 / N_{\rm e} N_{\rm e,+} \tag{21}$$

Thus, for systems consisting of short chains with a degree of polymerization $N_-\approx N_{\rm e}$, constraints imposed by the short chains on the long-chain motion disappear and the relaxation time of the longer chains is a reptation time in the super tube. For even smaller degrees of polymerization $N_- < N_{\rm e}$, short chains play the role of solvent diluting entanglements forming a super tube.

For polymer solutions of chains, the relationship between the degree of polymerization of the entangled strand $N_{\rm e}$, bond length l, Kuhn length b, and bead number density ρ is obtained from the Kavassalis—Noolandi conjecture. 45–47 In particular, one calculates the number of entangled strands, $P_{\rm e}$, with the degree of polymerization $N_{\rm e}$ within a confinement (tube) volume d_T^3 . Taking into account that strands within a confining volume are ideal with size $d_T \approx \sqrt{blN_{\rm e}}$, the number of

overlapping entangled strands inside the volume, d_T^3 , (packing number) is estimated as

$$P_{\rm e} \approx \rho d_T^3 / N_{\rm e} \approx \rho (bl)^{3/2} N_{\rm e}^{1/2}$$
 (22)

where ρ is the total bead density.

The degree of polymerization between entanglements, $N_{\rm e,+}$, associated only with the longer chains, $N_+=400$, forming a super tube, is different from $N_{\rm e}$ since these chains have a bead density ρ_+ . Substituting the density of monomers belonging to longer (positively charged) chains ρ_+ in eq 22 and assuming that the packing number remains the same, we arrive at the following expression for $N_{\rm e,+}$

$$N_{\rm e,+} \approx (\rho/\rho_{+})^2 N_{\rm e} \tag{23}$$

Thus, for the equal composition mixture of long and short chains, we should expect that $N_{\rm e,+}\approx 4N_{\rm e}$.

In our simulations, the primitive path analysis (PPA) ^{48,49} (see the Supporting Information for details) is used for calculations of $N_{\rm e}$ and $N_{\rm e,+}$. Since, for some systems, there are only a few entanglements per chain, $N_{\rm e}$ was obtained from analysis of the dependence of the mean-square end-to-end distance $\langle R_{\rm e}^2(s) \rangle$ of the primitive path chain with the bond length $l_{\rm pp}$ as a function of the number of bonds s. In particular, we calculated $N_{\rm e}$ from the primitive path Kuhn length, $N_{\rm e} = b_{\rm pp}/l_{\rm pp}$. Figure 5 shows the dependence of $\langle R_{\rm e}^2(s) \rangle / s l_{\rm pp}^2$ as a function of the number of bonds s in a primitive path segment. First, there is a linear increase with the number of bonds s followed by saturation at larger s values. The saturation corresponds to a crossover to the random walk regime of the primitive path. The plateau value is equal to the ratio of $b_{\rm pp}/l_{\rm pp}$ and thus defines the degree of polymerization of the entanglement strand. The analysis of the statistics of the

primitive path is quantified by fitting the simulation results to the following function 50

$$\langle R_{\rm e}^2(s) \rangle = s l_{\rm pp}^2 \left(\frac{1+A}{1-A} - \frac{2A}{s} \frac{1-A^s}{(1-A)^2} \right)$$
 (24)

where parameter $A=\langle\cos\theta\rangle$ is the average value of the bond angle between neighboring monomers along the primitive path. Note that, for this chain model, the ratio $b_{\rm pp}/l_{\rm pp}=(1+A)/(1-A)$, and in the limit $N_{\rm e}\gg 1$, eq 24 reduces to the expression for $\langle R_{\rm e}^2(s)\rangle$ of a semiflexible chain. This can be shown by substituting $A\approx 1-2/N_{\rm e}$ in eq 24. The results of this analysis are presented in Table 1 for all studied charged systems with $N_+=400$ and in the Supporting Information for neutral systems. The degree of polymerization between entanglements $N_{\rm e}$ increases with decreasing the bead concentration and decreases with increasing the chain Kuhn length. The observed trend is consistent with the entanglement dilution as the bead concentration decreases. These values of $N_{\rm e}$ are used to calculate the packing number $P_{\rm e}$ in accordance with eq 22. The obtained values for the packing number are between 16.7 and 19.5 (see Table 1), which are close to the values observed for polymer melts.

The data in Table 1 for charged polymers and the majority of data for neutral polymers (see the Supporting Information) for the entanglement degree of polymerization defining the tube and super tube follow universal scaling $N_{\rm e} \sim (\rho(lb)^{3/2})^{-2}$ with an average value of $P_{\rm e}=18.45\pm0.93$, as shown in Figure 6. However, for the data set of neutral chains with $\rho\sigma^3=0.85$,

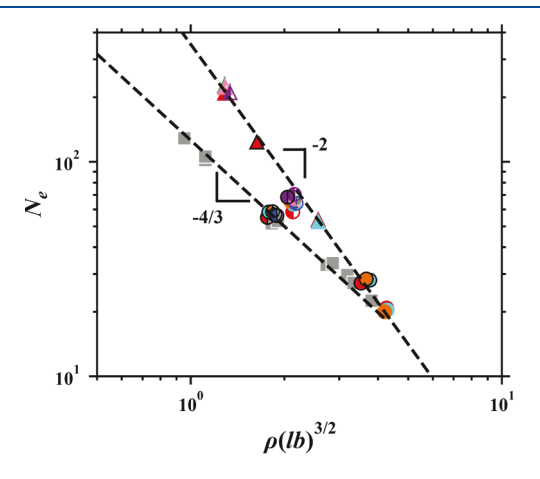


Figure 6. Degree of polymerization between entanglements $N_{\rm e}$ as a function of the dimensionless bead density $\rho(lb)^{3/2}$ for charged and neutral systems. Left-filled symbols correspond to super tubes in neutral and charged systems, and gray symbols correspond to systems of entangled ideal chains. Symbol notations are summarized in Table 1 and Tables S1 and S2. The dashed lines correspond to $N_{\rm e} = 353.4 \times (\rho(lb)^{3/2})^{-2}$ and $N_{\rm e} = 126.3 \times (\rho(lb)^{3/2})^{-4/3}$.

the degree of polymerization of the entanglement strands of the super tube was found to be located significantly below the line $N_{\rm e} \sim (\rho(lb)^{3/2})^{-2}$. To demonstrate that this super tube dilution follows the Rubinstein–Colby scaling ⁵⁴ for entanglements in a θ -solvent

$$P_{\rm e} \approx (\rho l^3 (b/l)^{3/4})^{2/3} N_{\rm e}^{1/2}$$
 (25)

we performed simulations of ideal phantom chains with N = 400, 800, and 1200 and the same Kuhn and bond lengths as neutral chains with interactions (see the Supporting

Information). To introduce entanglements between phantom chains, after system equilibration, we fixed the locations of the chains' ends and increased all interactions between beads from zero to full strength and at the same time decreased the chain bending constant to its bare value as those used in simulations of bimodal chain systems. This procedure fixed the topology of the chain trajectories, and the entanglements were analyzed by PPA. The results of this analysis are shown by the gray symbols in Figure 6. The best fit of the data to eq 25 gives the average $P_{\rm e} = 6.64 \pm 0.19$. Thus, in analyzing super tubes in mixtures of bimodal chains, it is important to consider the possibility of different scaling laws for tube dilution depending on the effective chain Kuhn length and concentration of the chains forming a super tube.

To highlight different chain's dynamics regimes, we calculated the mean-square displacement (MSD) of monomers 27,54 belonging to positively charged chains with $N_+=400$ averaged over 10 central beads

$$g_1(t) = \langle [r_i(t + \Delta t) - r_i(\Delta t)]^2 \rangle \tag{26}$$

to suppress fluctuations from the chain ends. Brackets $\langle ... \rangle$ in eq 26 correspond to the ensemble average over Δt . There are several scaling regimes of function $g_1(t)$. First, the regime with $g_1(t) \sim t$ corresponds to monomer diffusion at short time scales for time interval $t < \tau_0$ (τ_0 is the characteristic monomer relaxation time that depends on the interactions and surrounding environment). In the Rouse regime for strand dynamics between entanglements ($\tau_0 < t < \tau_e$), the function $g_1(t) \sim t^{1/2}$, and in the chain reptation regime ($\tau_e < t < \tau_R$), this function has weaker dependence on time $g_1(t) \sim t^{1/4}$.

These different regimes are shown in Figure 7a-d by plotting normalized $g_1(t)/t^{1/2}$ as a function of time t for systems of charged and neutral polymers. Specifically, in this representation, the crossover to the reptation regime appears as a decrease in the function $g_1(t)/t^{1/2}$ as a function of time. All data sets plotted in Figure 7 show similar trends. In particular, the function $g_1(t)/t^{1/2}$ first increases with time then passes through the maximum and then begins to decrease. For neutral systems with bead density $\rho \sigma^3 = 0.26$, we observe an increase in the function at later times, which is indicative of tube renewal dynamics. An increase in system density has a similar effect in both charged and neutral systems and is manifested in the slowdown of chains' dynamics caused by the renormalization of the monomeric friction coefficient due to electrostatic and excluded volume interactions and decreasing degree of polymerization of the entangled strands. Increasing the degree of polymerization of "polymeric counterions" results in flattening of the function at the intermediate time scales τ_0 < $t < \tau_{\rm e}$. For charged chains with $N_- > 50$ and bead density $\rho \sigma^3 =$ 0.85, there is a well-developed plateau. This is because the value of $N_{\rm e,+} \approx$ 80. However, for all other systems, function $g_1(t)/t^{1/2}$ passes through the maximum at this time scale. Therefore, it is problematic to use a crossover between regimes with $g_1(t) \sim t^{1/2}$ and $g_1(t) \sim t^{1/4}$ to accurately determine the tube diameter required for calculations of the degree of polymerization between entanglements, N_e . Note that the general trend in time dependence of the function $g_1(t)/t^{1/2}$ for charged systems is consistent with the results of ref 26.

Additional information about system dynamics is obtained from analysis of the mean-square displacement (MSD) of the center of mass^{27,54} (cm) of "counterion" chains with different degrees of polymerization

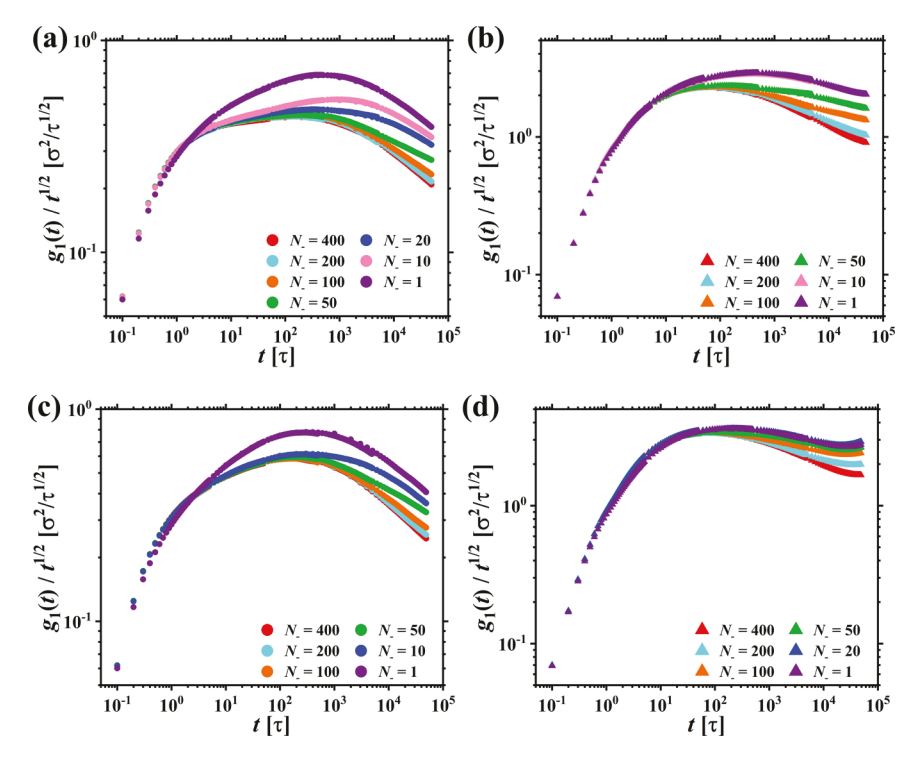


Figure 7. Mean-square displacement $g_1(t)$ averaged over 10 central monomers belonging to chains with N_+ = 400 in systems of charged chains with bead densities $\rho\sigma^3$ = 0.85 (a) and $\rho\sigma^3$ = 0.26 (b) and for systems of neutral chains with bead densities $\rho\sigma^3$ = 0.85 (c) and $\rho\sigma^3$ = 0.26 (d). Symbols of different color represent systems with polymeric counterions or solvent chains having DPs equal to 400 (red), 200 (light blue), 100 (orange), 50 (green), 20 (blue), 10 (pink), and 1 (purple).

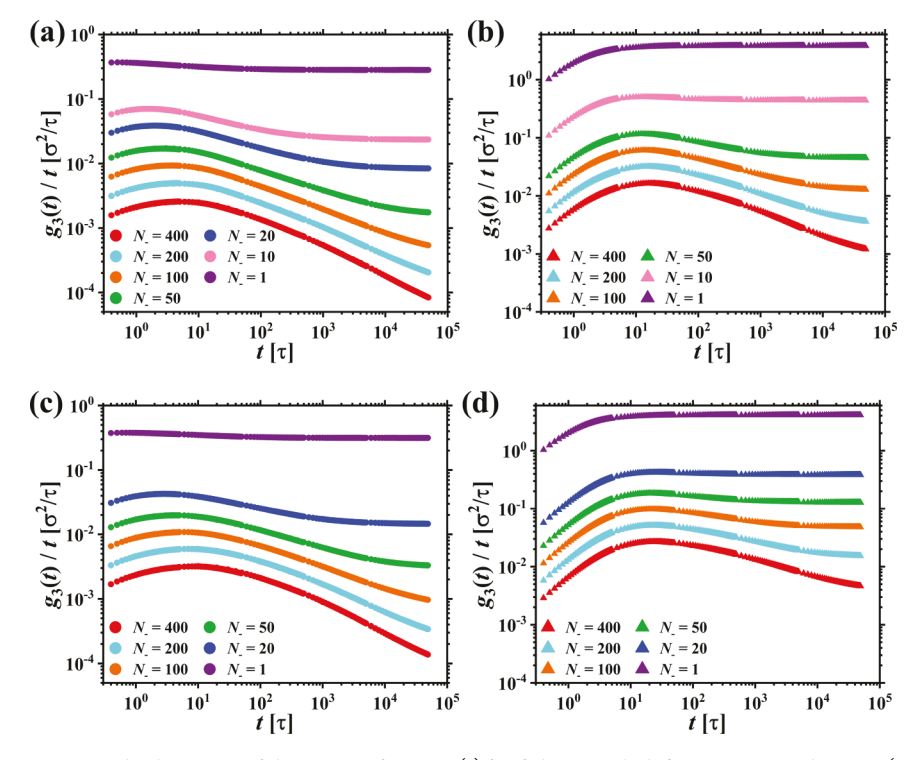


Figure 8. Normalized mean-square displacement of the center of mass $g_3(t)/t$ of chains with different DPs equal to 400 (red), 200 (light blue), 100 (orange), 50 (green), 20 (blue), 10 (pink), and 1 (purple) for systems of charged chains with bead densities $\rho\sigma^3 = 0.85$ (a) and $\rho\sigma^3 = 0.26$ (b) and for systems of neutral chains with bead densities $\rho\sigma^3 = 0.85$ (c) and $\rho\sigma^3 = 0.26$ (d).

$$g_{3}(t) = \langle [\mathbf{r}_{cm}(t + \Delta t) - \mathbf{r}_{cm}(\Delta t)]^{2} \rangle$$
(27)

Note that, for the chain center of mass motion of the entangled chains with N_{-} = 400, the different time regimes of

the function $g_1(t)$ discussed above correspond to the scaling regimes of function $g_3(t) \sim t$, $t^{1/2}$, and t. At time scales longer than the chain relaxation time, functions $g_1(t)$ and $g_3(t)$ converge and increase linearly with time $g_1(t) \approx g_3(t) \sim t$. ⁵⁴

Figure 8a-d shows the normalized function $g_3(t)/t$ as a function of time for "counterions" with DPs equal to 1, 10, 20, 50, 100, 200, and 400 for charged systems and for solvent chains with DPs equal to 1, 20, 50, 100, 200, and 400 for neutral systems. The plateau regime at longer times corresponds to diffusive motion with the diffusion coefficient being equal to the plateau value. For polymeric counterions or solvents, there is a characteristic peak at short time scales whose location and magnitude depend on the degree of polymerization. This corresponds to monomer exploration of the surrounding environment. The decrease in $g_3(t)/t$ reflects contributions from the Rouse modes to the chain center of mass dynamics at intermediate time scales. One can collapse different curves by using the locations and magnitudes of the maxima as normalization factors, as demonstrated in the Supporting Information. A deviation from the universal curve at later times is observed for entangled chains in both types of systems consisting of charged and neutral chains. Note that the observed plateau values for short chains are not simple multiples of the DPs due to the chain ends effect.

CONCLUSIONS

We study the static and dynamic properties of concentrated polyelectrolyte solutions and mixtures of oppositely charged chains. For the studied bead (monomer) concentrations, the electrostatic interactions are screened, which is manifested in a relatively weak renormalization of the chain Kuhn length (see Table 1) and a moderate increase in the chain size in comparison with the reference system of neutral chains. However, the presence of electrostatic interactions and requirements of system electroneutrality at the large length scale result in the appearance of a peak in the static structure factor S(q) in which the position moves toward smaller q values with decreasing bead concentrations, as shown in Figure 4. The value of the plateau at a small q increases with decreasing bead concentration (increasing system compressibility) and increasing degree of polymerization of negatively charge chains ("polymeric" counterions). The largest suppression of fluctuations at $q \rightarrow 0$ is observed for polyelectrolyte solutions with monovalent counterions. Comparison of simulation results with RPA calculations of the scattering function points out the strong effect of fluctuations in the renormalization of the bare system parameters.

Chains' dynamics in polyelectrolyte solutions and in mixtures of oppositely charged chains also show subtle differences. In particular, in polyelectrolyte solutions, the degree of polymerization between entanglements N_e is about 4 times of that in symmetric mixtures of oppositely charged chains and is comparable with the values obtained in systems of neutral chains with monomeric solvents (see Table 1 and Table S1). The increasing degree of polymerization of the negatively charged chains increases the concentration of entanglements per chain due to the decrease in N_e . In the mixtures of chains with two different degrees of polymerization, in addition to chain reptation, there is a constraint release (disentanglements of short chains from long ones) that shortens the longer chain reptation time, as illustrated in Figures 7 and 8. The observed trends are similar for systems of both charged and neutral chains. For studied bead concentrations, the effect of the electrostatic interactions on chain's dynamics can be reduced to renormalization of the monomeric friction coefficient and Kuhn length that are responsible for rescaling of the chains' dynamics. 25,26 Our simulation results

could provide the foundation for future development of the scaling theory of dynamics in solutions of charged polymers. ^{22,55}

ASSOCIATED CONTENT

5 Supporting Information

The Supporting Information is available free of charge at https://pubs.acs.org/doi/10.1021/acs.macromol.1c01171.

Simulation details, random phase approximation calculations of the static structure factor, analysis of the chain reptation dynamics, and entanglements (PDF)

AUTHOR INFORMATION

Corresponding Author

Andrey V. Dobrynin — Department of Chemistry, University of North Carolina, Chapel Hill, North Carolina 27599, United States; orcid.org/0000-0002-6484-7409; Email: avd@email.unc.edu

Authors

Ryan Sayko — Department of Chemistry, University of North Carolina, Chapel Hill, North Carolina 27599, United States; orcid.org/0000-0002-5986-4829

Yuan Tian — Department of Chemistry, University of North Carolina, Chapel Hill, North Carolina 27599, United States; ocid.org/0000-0002-7277-1408

Heyi Liang — Pritzker School of Molecular Engineering, University of Chicago, Chicago, Illinois 60637, United States; © orcid.org/0000-0002-8308-3547

Complete contact information is available at: https://pubs.acs.org/10.1021/acs.macromol.1c01171

Note

The authors declare no competing financial interest.

ACKNOWLEDGMENTS

This work was supported by the National Science Foundation under the grant DMREF-2049518.

REFERENCES

- (1) Katchalsky, A. Polyelectrolytes. Pure Appl. Chem. **1971**, 26, 327–374.
- (2) de Gennes, P. G.; Pincus, P.; Brochard, F.; Velasco, R. M.; Brochard, F. Remarks on polyelectrolyte conformation. *J. Phys. France* **1976**, *37*, 1461–1473.
- (3) Förster, S.; Schmidt, M. Polyelectrolytes in Solution. *Adv. Polym. Sci.* 1995, 120, 51–133.
- (4) Borue, V. Y.; Erukhimovich, I. Y. A Statistical theory of weakly charged polyelectrolytes: Fluctuations, equation of state, and microphase separation. *Macromolecules* **1988**, *21*, 3240–3249.
- (5) Dobrynin, A. V.; Rubinstein, M. Theory of polyelectrolytes in solutions and at surfaces. *Prog. Polym. Sci.* **2005**, *30*, 1049–1118.
- (6) Grosberg, A. Y.; Nguyen, T. T.; Shklovskii, B. I. Colloquium: The physics of charge inversion in chemical and biological systems. *Rev. Mod. Phys.* **2002**, *74*, 329–345.
- (7) Muthukumar, M. 50th Anniversary Perspective: A Perspective on polyelectrolyte solutions. *Macromolecules* **2017**, *50*, 9528–9560.
- (8) Perry, S. L.; Sing, C. E. 100th anniversary of macromolecular science viewpoint: Opportunities in the physics of sequence-defined polymers. *ACS Macro Lett.* **2020**, *9*, 216–225.
- (9) Sing, C. E. Development of the modern theory of polymeric complex coacervation. Adv. Colloid Interface Sci. 2017, 239, 2–16.

- (10) Rumyantsev, A. M.; Jackson, N. E.; Pablo, J. J. d. Polyelectrolyte complex coacervates: Recent developments and new frontiers. *Annu. Rev. Condens. Matter Phys.* **2021**, *12*, 155–176.
- (11) Borue, V. Y.; Erukhimovich, I. Y. A statistical theory of globular polyelectrolyte complexes. *Macromolecules* **1990**, *23*, 3625–3632.
- (12) de la Cruz, M. O.; Belloni, L.; Delsanti, M.; Dalbiez, J. P.; Spalla, O.; Drifford, M. Precipitation of highly charged polyelectrolyte solutions in the presence of multivalent salts. *J. Chem. Phys.* **1995**, *103*, 5781–5791.
- (13) Huang, C.-I.; de la Cruz, M. Polyelectrolytes in multivalent salt solutions: Monomolecular versus multimolecular aggregation. *Macromolecules* **2002**, *35*, 976–986.
- (14) Solis, F. J.; de la Cruz, M. O. Collapse of flexible polyelectrolytes in multivalent salt solutions. *J. Chem. Phys.* **2000**, *112*, 2030–2035.
- (15) Gucht, J. v. d.; Spruijt, E.; Lemmers, M.; Cohen Stuart, M. A. Polyelectrolyte complexes: Bulk phases and colloidal systems. *J. Colloid Interface Sci.* **2011**, *361*, 407–422.
- (16) Rubinstein, M.; Liao, Q.; Panyukov, S. Structure of liquid coacervates formed by oppositely charged polyelectrolytes. *Macromolecules* **2018**, *51*, 9572–9588.
- (17) Rubinstein, M.; Colby, R. H.; Dobrynin, A. V. Dynamics of semidilute polyelectrolyte solutions. *Phys. Rev. Lett.* **1994**, 73, 2776—2779.
- (18) Dobrynin, A. V.; Colby, R. H.; Rubinstein, M. Scaling theory of polyelectrolyte solutions. *Macromolecules* **1995**, *28*, 1859–1871.
- (19) Colby, R. H. Structure and linear viscoelasticity of flexible polymer solutions: comparison of polyelectrolyte and neutral polymer solutions. *Rheol. Acta* **2010**, *49*, 425–442.
- (20) Dobrynin, A. V., Polyelectrolyte Solutions and Gels. In *Oxford Handbook of Soft Matter*; Terentjev, E.; Weitz, D., Eds. Oxford University Press: Oxford, 2015; pp. 269–344.
- (21) Syed, V. M. S.; Srivastava, S. Time-ionic strength superposition: A unified description of chain relaxation dynamics in polyelectrolyte complexes. *ACS Macro Lett.* **2020**, *9*, 1067–1073.
- (22) Dobrynin, A. V.; Jacobs, M. When do polyelectrolytes entangle? *Macromolecules* **2021**, *54*, 1859–1869.
- (23) Han, A.; Colby, R. H. Rheology of entangled polyelectrolyte solutions. *Macromolecules* **2021**, *54*, 1375–1387.
- (24) Delaney, K. T.; Fredrickson, G. H. Theory of polyelectrolyte complexation—Complex coacervates are self-coacervates. *J. Chem. Phys.* **2017**, *146*, 224902.
- (25) Liao, Q.; Carrillo, J. M. Y.; Dobrynin, A. V.; Rubinstein, M. Rouse dynamics of polyelectrolyte solutions: Molecular dynamics study. *Macromolecules* **2007**, *40*, 7671–7679.
- (26) Yu, B.; Rauscher, P. M.; Jackson, N. E.; Rumyantsev, A. M.; de Pablo, J. J. Crossover from Rouse to reptation dynamics in salt-free polyelectrolyte complex coacervates. *ACS Macro Lett.* **2020**, *9*, 1318–1324
- (27) Kremer, K.; Grest, G. S. Dynamics of entangled linear polymer melts: A molecular-dynamics simulation. *J. Chem. Phys.* **1990**, *92*, 5057–5086.
- (28) Carrillo, J.-M. Y.; Dobrynin, A. V. Polyelectrolytes in salt solutions: molecular dynamics simulations. *Macromolecules* **2011**, *44*, 5798–5816.
- (29) Gubarev, A.; Carrillo, J.-M. Y.; Dobrynin, A. V. Scale-dependent electrostatic stiffening in biopolymers. *Macromolecules* **2009**, *42*, 5851–5860.
- (30) de Gennes, P. G. Theory of X-ray scattering by liquid macromolecules with heavy atom labels. *J. Phys. France* **1970**, *31*, 235–238
- (31) de Gennes, P. G. Theory of long-range correlations in polymer melts. *Faraday Discuss. Chem. Soc.* **1979**, *68*, 96–103.
- (32) Leibler, L.; Benoit, H. Theory of Correlations in Partly Labelled Homopolymer Melts. *Polymer* **1981**, *22*, 195–201.
- (33) Yerukhimovich, I. Y. Effect of chemical structure of two-component melts of heteropolymers on the formation of domain structure. *Polym. Sci. U.S.S.R* **1982**, *24*, 2232–2241.

- (34) Fredrickson, G. H.; Helfand, E. Fluctuation effects in the theory of microphase separation in block copolymers. *J. Chem. Phys.* **1987**, 87, 697–705.
- (35) Mayes, A. M.; de la Cruz, M. O. Concentration fluctuation effects on disorder-order transitions in block copolymer melts. *J. Chem. Phys.* **1991**, 95, 4670–4677.
- (36) Dobrynin, A. V.; Erukhimovich, I. Y. Fluctuation effects in the theory of weak supercrystallization in block copolymer systems of complicated chemical structure. *J. Phys. II* **1991**, *1*, 1387–1404.
- (37) Liang, H.; Wang, Z.; Dobrynin, A. V. Scattering from melts of combs and bottlebrushes: Molecular dynamics simulations and theoretical study. *Macromolecules* **2019**, *52*, 5555–5562.
- (38) Dobrynin, A. V.; Erukhimovich, I. Y. Weak crystallization and structural phase transitions in weakly charged polyelctrolyte systems. *Zh. Eksp. Teor. Fiz.* **1991**, *99*, 1344–1359.
- (39) Brazovskii, S. A. Phase transition of an isotropic system to a nonuniform state. Sov. J. Exp. Theor. Phys. 1996, 11, 109–113.
- (40) Viovy, J. L.; Rubinstein, M.; Colby, R. H. Constraint release in polymer melts: Tube reorganization versus tube dilation. *Macromolecules* **1991**, *24*, 3587–3596.
- (41) Rubinstein, M.; Colby, R. H. Self-consistent theory of polydisperse entangled polymers: Linear viscoelasticity of binary blends. *J. Chem. Phys.* **1988**, *89*, 5291–5306.
- (42) Picu, R. C.; Rakshit, A. Coarse grained model of diffusion in entangled bidisperse polymer melts. J. Chem. Phys. 2007, 127, 144909.
- (43) Wang, Z.; Larson, R. G. Constraint release in entangled binary blends of linear polymers: A molecular dynamics study. *Macromolecules* **2008**, *41*, 4945–4960.
- (44) Larson, R. G.; Sridhar, T.; Leal, L. G.; McKinley, G. H.; Likhtman, A. E.; McLeish, T. C. B. Definitions of entanglement spacing and time constants in the tube model. *J. Rheol.* **2003**, *47*, 809–818.
- (45) Kavassalis, T. A.; Noolandi, J. New view of entanglements in dense polymer systems. *Phys. Rev. Lett.* **1987**, *59*, 2674–2677.
- (46) Kavassalis, T. A.; Noolandi, J. A new theory of entanglements and dynamics in dense polymer systems. *Macromolecules* **1988**, *21*, 2869–2879.
- (47) Kavassalis, T. A.; Noolandi, J. Entanglement scaling in polymer melts and solutions. *Macromolecules* **1989**, *22*, 2709–2720.
- (48) Everaers, R.; Sukumaran, S. K.; Grest, G. S.; Svaneborg, C.; Sivasubramanian, A.; Kremer, K. Rheology and microscopic topology of entangled polymeric liquids. *Science* **2004**, *303*, 823–826.
- (49) Sukumaran, S. K.; Grest, G. S.; Kremer, K.; Everaers, R. Identifying the primitive path mesh in entangled polymer liquids. *J. Polym. Sci., Part B: Polym. Phys.* **2005**, 43, 917–933.
- (50) Grosberg, A. Y.; Khokhlov, A. R., Statistical Physics of Macromolecules; AIP Press: 1994.
- (51) Milner, S. T. Unified entanglement scaling for flexible, semiflexible, and stiff polymer melts and solutions. *Macromolecules* **2020**, 53, 1314–1325.
- (52) Bobbili, S. V.; Milner, S. T. Simulation study of entanglement in semiflexible polymer melts and solutions. *Macromolecules* **2020**, *53*, 3861–3872.
- (53) Rubinstein, M.; Colby, R. H. Polymer Physics; Oxford University Press: New York, NY, 2003.
- (54) Doi, M.; Edwards, S. F. The Theory of Polymer Dynamics; Oxford University Press: 1986.
- (55) Aponte-Rivera, C.; Rubinstein, M. Dynamic coupling in unentangled liquid coacervates formed by oppositely charged polyelectrolytes. *Macromolecules* **2021**, *54*, 1783–1800.